AIP Applied Physics Letters

High-endurance megahertz electrical self-oscillation in Ti/NbO x bilayer structures

Shuai Li, Xinjun Liu, Sanjoy Kumar Nandi, Dinesh Kumar Venkatachalam, and Robert Glen Elliman

Citation: Applied Physics Letters **106**, 212902 (2015); doi: 10.1063/1.4921745
View online: http://dx.doi.org/10.1063/1.4921745
View Table of Contents: http://scitation.aip.org/content/aip/journal/apl/106/21?ver=pdfcov
Published by the AIP Publishing

Articles you may be interested in
Atomic structures and electronic properties of 2H-NbSe2: The impact of Ti doping
J. Appl. Phys. **116**, 103709 (2014); 10.1063/1.4895489

Preparation of overdamped NbTiN Josephson junctions with bilayered Ti–TiN barriers
J. Appl. Phys. **108**, 113904 (2010); 10.1063/1.3517475

Nanotwins and phases in high-strain Pb (Mg 1 / 3 Nb 2 / 3) 1 − x Ti x O 3 crystal
J. Appl. Phys. **103**, 074117 (2008); 10.1063/1.2904900

Structures and dielectric properties of Bi 1.5 Zn 1.0 Nb 1.5 − x Ti x O 7 (x = 0 , 0.05, and 0.10) thin films
Appl. Phys. Lett. **90**, 042903 (2007); 10.1063/1.2433762

Dielectric, domain, and optical studies in high-Curie-temperature Pb (In 1∕2 Nb 1∕2) 1 − x Ti x O 3 (x = 0.40) single crystal
J. Appl. Phys. **100**, 104104 (2006); 10.1063/1.2387140

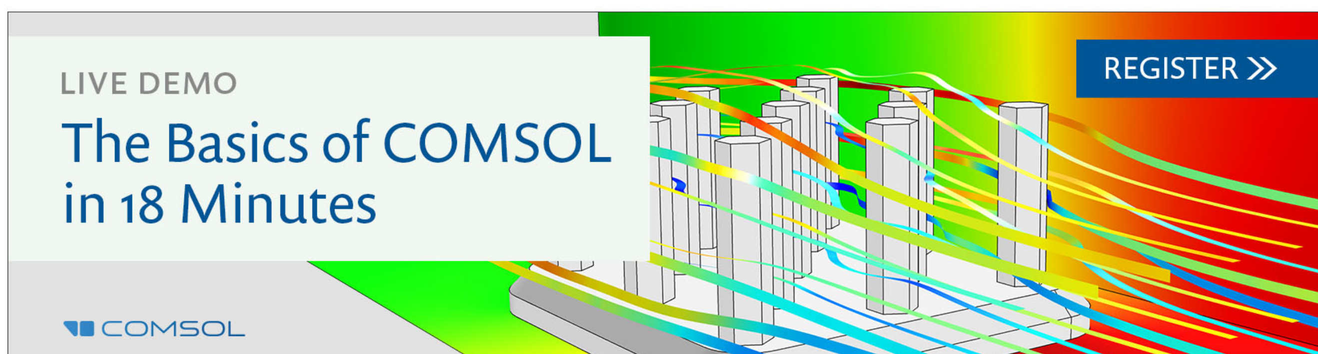

This article is copyrighted as indicated in the article. Reuse of AIP content is subject to the terms at: http://scitation.aip.org/termsconditions. Downloaded to IP: 130.56.107.13 On: Tue, 21 Jul 2015 08:47:01

APPLIED PHYSICS LETTERS **106**, 212902 (2015)

High-endurance megahertz electrical self-oscillation in Ti/NbO_x bilayer structures

Shuai Li,[1] Xinjun Liu,[1,a)] Sanjoy Kumar Nandi,[1,2,3] Dinesh Kumar Venkatachalam,[1] and Robert Glen Elliman[1,b)]

[1]*Department of Electronic Materials Engineering, Research School of Physics and Engineering, The Australian National University, Canberra, ACT 0200, Australia*
[2]*Research School of Astronomy and Astrophysics, The Australian National University, Canberra, ACT 0200, Australia*
[3]*Department of Physics, University of Chittagong, Chittagong-4331, Bangladesh*

(Received 1 April 2015; accepted 14 May 2015; published online 26 May 2015)

Electrical self-oscillation is reported for a Ti/NbO_x negative differential resistance device incorporated in a simple electric circuit configuration. Measurements confirm stable operation of the oscillator at source voltages as low as 1.06 V, and demonstrate frequency control in the range from 2.5 to 20.5 MHz for voltage changes as small as $\sim$1 V. Device operation is reported for $>6.5 \times 10^{10}$ cycles, during which the operating frequency and peak-to-peak device current decreased by $\sim$25%. The low operating voltage, large frequency range, and high endurance of these devices makes them particularly interesting for applications such as neuromorphic computing. *© 2015 AIP Publishing LLC*. [http://dx.doi.org/10.1063/1.4921745]

Transition metal oxides which exhibit a metal-insulator transition (MIT) (e.g., VO_2, NbO_2, Ti_2O_3) are of particular scientific and technological interest, and have found wide spread application as functional materials.[1–4] This stems from the fact that the MIT can be controlled by external stimuli (e.g., temperature, pressure, and electric field) and results in abrupt changes in the materials intrinsic properties (e.g., electrical conductivity, thermal conductivity, and refractive index).[3–5] In this context, vanadium dioxide (VO_2) is one of the most well studied and widely exploited materials.[5] It undergoes a thermally induced insulator-metal transition at a temperature of 340 K. Of particular relevance to the present study is the use of VO_2 films as the active element in relaxation oscillators. This application derives from the fact that the MIT can be induced in a simple metal/VO_2/metal structure by Joule heating, and the fact that such structures exhibit current-controlled negative differential resistance (NDR). The resulting oscillators have been shown to operate at frequencies in the range from 1 kHz to 1 MHz.[6,7]

Unfortunately, the low MIT temperature of VO_2 precludes its use in many microelectronics applications where the expectation is that devices will operate at temperature approaching 400 K. To address this limitation recent interest has been focussed on materials with higher transition temperatures, including NbO_2 which has a transition temperature of $\sim$1080 K.[8,9] Studies have demonstrated the potential of NbO_2 for applications in optical modulation,[10] electrical switching,[11] and memory devices.[12,13] Recently, the MIT-induced oscillation phenomenon has been reported in NbO_x with sub-nanosecond switching speed and $\sim$100 fJ switching energies.[14] The properties of these MIT-induced oscillators make them suitable for applications such as voltage-controlled oscillators,[15,16] electronic switches,[17,18] neuristor,[19] and nano-oscillator based non-boolean associative architectures.[20–22] In this study, NbO_x based relaxation oscillators are reported with high-endurance operation at frequencies up to $\sim$20 MHz.

Simple metal/oxide/metal test structures were employed for the current study. An insulating layer (150 nm SiN_x) was first deposited on a silicon substrate by plasma enhanced chemical vapour deposition (PECVD) to isolate the test structure from the silicon substrate. A 50 nm thick Pt layer was then deposited by electron beam evaporation to form the bottom electrode. The active niobium oxide layer was then deposited onto the bottom electrode by reactively sputter deposition using a metallic Nb source and an O_2/Ar gas mixture in the ratio of 1/9. The film thickness was 85 nm as verified by ellipsometry. Top electrodes consisting of a 10 nm Ti layer and a 50 nm Pt layer were then deposited through a shadow mask by electron beam evaporation to produce an array of circular contacts of 150 μm diameter. These structures were subsequently annealed by rapid thermal annealing (RTA) at 300 °C for 300 s under Ar gas flow. Electrical characterization was undertaken with an Agilent B1500A parametric analyser.

Fig. 1 shows typical DC current-voltage (I-V) characteristics of devices during voltage-controlled (Fig. 1(a)) and current-controlled (Fig. 1(b)) sweeps. The former shows threshold switching behaviour, in which the oxide layer transforms to a metallic state as the voltage is increased beyond a threshold value and returns to an insulating state as it is reduced below a critical hold voltage. In this case, the MIT is believed to result from Joule heating of a filamentary conduction path in the oxide layer,[14] a mechanism that is supported by its nonpolar nature, which is illustrated in the inset of Fig. 1(a). In this context, it should be noted that threshold switching is only observed after an initial forming process, in which the voltage is scanned from 0 to -8 V.[23]

The current-controlled I-V sweep (Fig. 1(b)) provides additional insight into the switching process, and clearly highlights the NDR response of these devices. This was measured by scanning the current from 0 mA to 5 mA and

a)Electronic mail: xinjun.liu@anu.edu.au
b)Electronic mail: rob.elliman@anu.edu.au

 © 2015 AIP Publishing LLC

This article is copyrighted as indicated in the article. Reuse of AIP content is subject to the terms at: http://scitation.aip.org/termsconditions. Downloaded to IP: 130.56.107.13 On: Tue, 21 Jul 2015 08:47:01

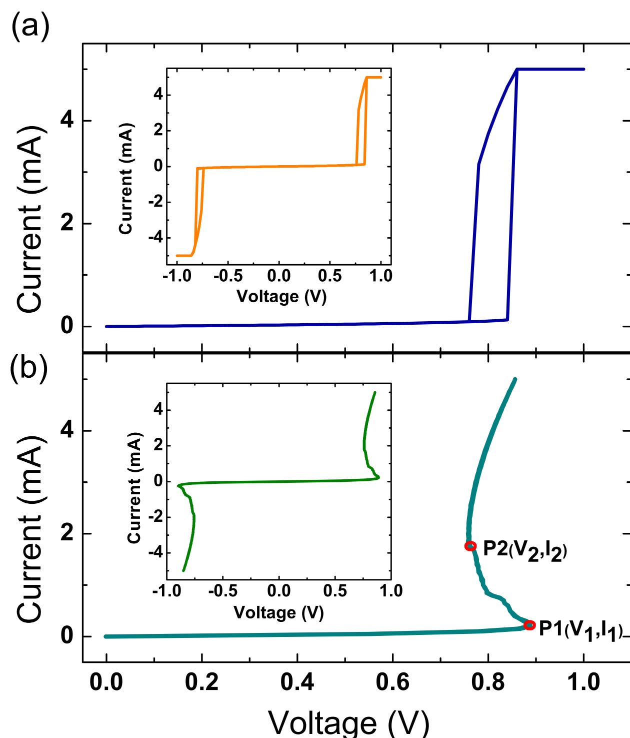

FIG. 1. Typical current-voltage characteristics of the device, (a) positive voltage sweep and (b) positive current sweep. Insets show symmetric, non-polar nature of voltage and current sweeps.

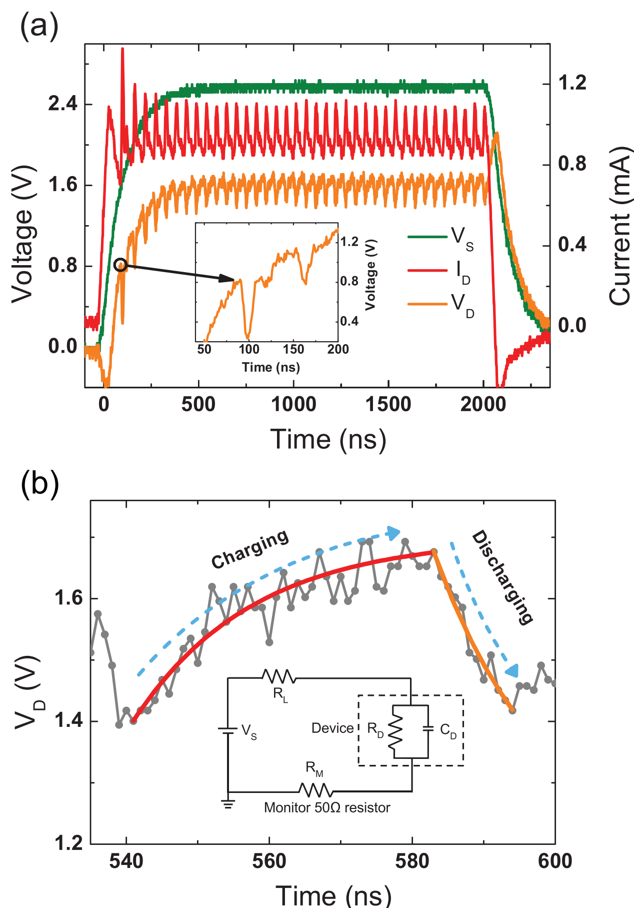

FIG. 2. (a) Electrical oscillatory responses of V_D and I_D during a 2 μs 2.6 V pulse. Inset shows detail of the initial response. (b) Expanded view of a single device voltage oscillation. Inset shows the equivalent circuit used for analysis.

back to 0 mA in 50 μA steps. The current and voltage at P1 and P2 were measured as ~0.3 mA and ~0.88 V and ~1.95 mA and ~0.76 V, respectively, where V_1 and V_2 are known as threshold and hold voltages. The symmetric, non-polar nature of the characteristics is again highlighted in the inset. This NDR response provides the basis for a relaxation oscillator and is the focus of the following discussion.[24]

The oscillation dynamics of NbO_x devices were studied by including the devices in a series circuit, as shown in the inset of Fig. 2(b). The circuit consists of a source voltage (V_S), a load resistor (R_L), a 50 Ω monitoring resistor (R_M) and the device under test. Rectangular voltage pulses were generated with a Waveform Generator/Fast Measurement Unit (WGFMU) as part of the B1500A analyser, and the resulting electrical response was recorded by monitoring the voltage drop across the 50 Ω resistor using a Tektronix TPS2024B oscilloscope.

Fig. 2(a) shows the device voltage (V_D) and current I_D during excitation with a pulse of amplitude of 2.6 V and width of 2 μs, with R_L equal to 1 kΩ. Oscillations begin as V_D reaches ~0.82 V, as illustrated in the inset of Fig. 2(a), which is close to the threshold voltage reported in Fig. 1(b). Stable, periodic oscillations are observed once V_S reaches its specified value of 2.6 V. For this case, the peak-to-peak amplitudes were measured as ~0.3 V and ~0.26 mA, respectively. The oscillation frequency was determined from fast Fourier transform analysis to be 19 MHz.

The oscillator circuit depicted in Fig. 2(b) is of the Pearson-Anson form and its response is determined by the device NDR characteristics (Fig. 1(b)) and by V_S and R_L.[25] Each oscillation of I_D and V_D shows an exponential rise and fall, similar to that previously reported for VO_2.[6] This is illustrated in Fig. 2(b) and can be modelled from the equivalent RC circuit shown in the inset. The time constant for charging is given by RC, where C is the device capacitance, estimated to be ~15 pF, and $R_{eff} = (R_L + R_M)R_D/(R_L + R_M + R_D)$ with R_D representing the high resistance state of the NbO_x device. The time constant for charging was ~42 ns in this case. As V_D approaches its maximum value, the device switches to its low resistance state and V_D begins to drop with an RC time constant, in which R_D now represents the low resistance state of the device. The discharging time constant was ~11 ns.

Fig. 3(a) depicts the oscillation range of V_S and R_L, and compares values determined from direct measurement with those derived from the data in Fig. 1(b) using load-line analysis.[24] The region bounded by the solid lines represents V_S and R_L values for which stable oscillation was observed. This shows that stable oscillations were observed at source voltage as low as 1.06 V for R_L equal to 0.5 kΩ, which corresponds to a peak device voltage of 0.9 V. Also shown, color-coded is the effect of these parameters on the oscillation frequency. This shows that the frequency increases with increasing voltage for a given load resistance. This is shown more explicitly in Fig. 3(b), which also demonstrates the near linear scaling of frequency with V_S. This dependence is consistent with that expected for the Pearson-Anson oscillator, as shown in the inset of Fig. 2(b), which predicts a dependence of the form[24]

This article is copyrighted as indicated in the article. Reuse of AIP content is subject to the terms at: http://scitation.aip.org/termsconditions. Downloaded to IP: 130.56.107.13 On: Tue, 21 Jul 2015 08:47:01

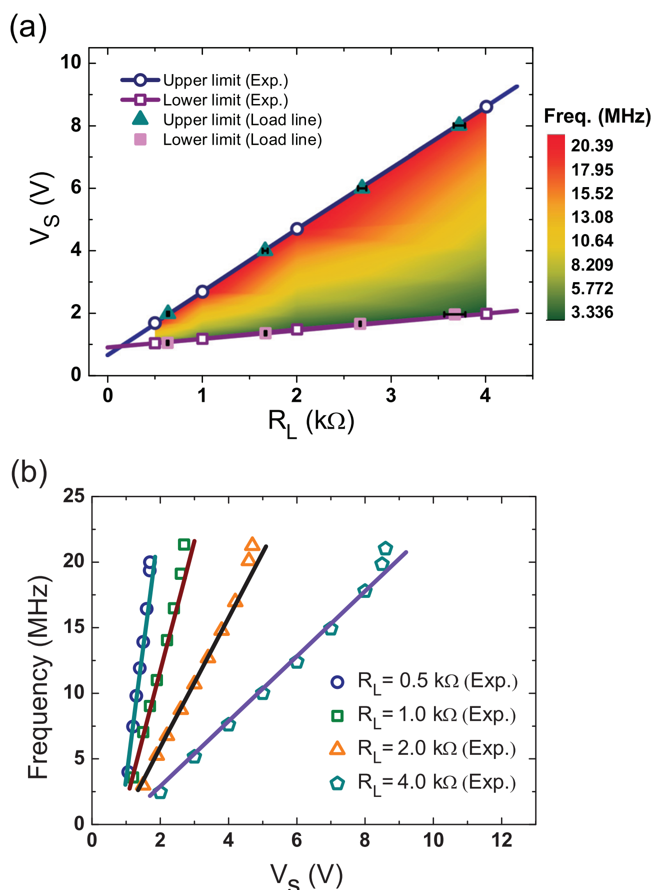

FIG. 3. (a) Oscillation window defined by V_S and R_L with oscillation frequency depicted by shading. (b) Oscillation frequency as a function of V_S for different values of R_L. Solid lines represent fits of Eq. (1).

$$f_o = \left[\alpha R_L C \ln\left(\frac{V_S - V_2}{V_S - V_1}\right)\right]^{-1}, \quad (1)$$

where V_1 and V_2 are the threshold and hold voltages, and α is a scaling parameter, which accounts for factors such as parasitic capacitance. The solid lines in Fig. 3(b) represent a fit of this equation to the data with a fixed α value of 55 for all curves.

Device endurance and stability are important for practical applications. These were tested by running oscillators for 96 min with a pulse amplitude of 2.2 V, which corresponds to $\sim 6.5 \times 10^{10}$ oscillation cycles. The oscillation characteristics were monitored after 1, 6, 36, and 96 min by recording the oscillator output. The stability of the peak-to-peak device current and oscillation frequency are shown in Fig. 4. The peak-to-peak current is observed to undergo a 20% reduction in amplitude during the first $\sim 8 \times 10^8$ (1 min) cycles but to remain reasonably constant thereafter. In contrast, the oscillation frequency decreases almost linearly with increasing cycle number, decreasing by around 25% over the full testing period, $\sim 6.5 \times 10^{10}$ cycles. The relative changes in the peak-to-peak current and frequency are similar ($\sim$25%) over the full testing period, but their trend with increasing cycle number is clearly quite different. The only variables in the circuit, once V_S and R_L are fixed, are the device capacitance and resistance. It is therefore clear that the device structure changes with time during continuous operation.

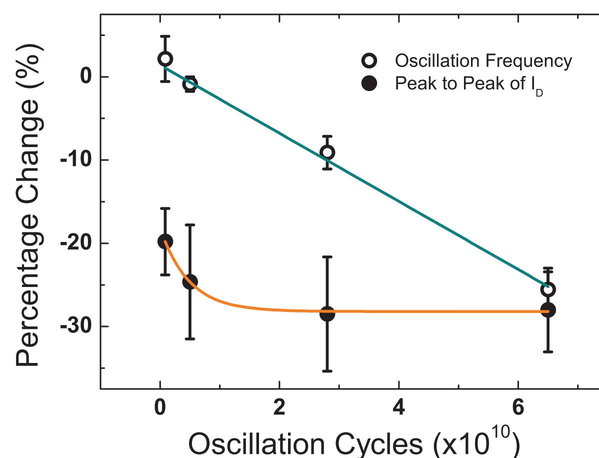

FIG. 4. Change in oscillation frequency and peak-to-peak amplitude as a function of oscillation cycle number. The data points represent measurements after 1, 6, 36, and 96 min.

For the simple equivalent circuit depicted in Fig. 2(b), the device current depends only on changes in the device resistance, while the frequency is affected by changes in both the resistance and capacitance. While it is possible to construct schemes where specific changes in resistance and capacitance account for the changes reported in Fig. 4, this remains speculative and further work is required to understand the physical changes occurring in the device. Given the relatively high temperature of the MIT such changes are likely to result from Joule-heating induced chemical reactions at the NbO_x/Ti interface or modification of the MIT volume.

In conclusion, we have investigated the properties of a relaxation oscillator based on the metal-insulator transition in NbO_2. The parameters (load resistance and source voltage) required for stable oscillation were shown to be consistent with the NDR response of isolated devices, and the oscillation frequency was shown to scale linearly with source voltage (for a given load resistance), as predicted for a Pearson-Anson oscillator. Measurements confirmed stable operation of the oscillator at source voltages as low as 1.06 V, and demonstrated frequency control in the range from 2.5 to 20.5 MHz for voltage changes as small as $\sim$1 V. Devices operated for $\sim 6.5 \times 10^{10}$ cycles during which their frequency and peak-to-peak current decreased by $\sim$25%. The low operating voltage, large frequency range, and high endurance of these devices makes them particularly interesting for applications such as neuromorphic computing.

This work was made possible by funding from the Australian Research Council. We would also like to acknowledge and thank Australian Nanotechnology Fabrication Facility (ANFF) ACT node for their research facility.

[1]D. Kuzum, S. Yu, and H.-S. P. Wong, Nanotechnology **24**, 382001 (2013).
[2]H.-S. Wong, H.-Y. Lee, S. Yu, Y.-S. Chen, Y. Wu, P.-S. Chen, B. Lee, F. Chen, and M.-J. Tsai, Proc. IEEE **100**, 1951–1970 (2012).
[3]Z. Yang, C. Ko, and S. Ramanathan, Annu. Rev. Mater. Res. **41**, 337–367 (2011).
[4]S. D. Ha and S. Ramanathan, J. Appl. Phys. **110**, 071101 (2011).
[5]S. Ha, Y. Zhou, A. Duwel, D. White, and S. Ramanathan, IEEE Microwave Mag. **15**, 32–44 (2014).

This article is copyrighted as indicated in the article. Reuse of AIP content is subject to the terms at: http://scitation.aip.org/termsconditions. Downloaded to IP: 130.56.107.13 On: Tue, 21 Jul 2015 08:47:01

[6]Y. W. Lee, B.-J. Kim, J.-W. Lim, S. J. Yun, S. Choi, B.-G. Chae, G. Kim, and H.-T. Kim, Appl. Phys. Lett. **92**, 162903 (2008).
[7]A. Beaumont, J. Leroy, J.-C. Orlianges, and A. Crunteanu, J. Appl. Phys. **115**, 154502 (2014).
[8]R. Janninck and D. Whitmore, J. Phys. Chem. Solids. **27**, 1183–1187 (1966).
[9]D. Adler, Rev. Mod. Phys. **40**, 714–736 (1968).
[10]J. C. Lee and W. W. Durand, J. Appl. Phys. **56**, 3350 (1984).
[11]H. R. Philipp and L. M. Levinson, J. Appl. Phys. **50**, 4814 (1979).
[12]S. Kim, X. Liu, J. Park, S. Jung, W. Lee, J. Woo, J. Shin, G. Choi, C. Cho, S. Park, D. Lee, E. Jun Cha, B.-H. Lee, H. D. Lee, S. G. Kim, S. Chung, and H. Hwang, Symp. VLSI Technol. **2012**, pp. 155–156.
[13]X. Liu, S. Nandi, D. Venkatachalam, K. Belay, S. Song, and R. Elliman, IEEE Electron Device Lett. **35**, 1055–1057 (2014).
[14]M. D. Pickett and R. S. Williams, Nanotechnology **23**, 215202 (2012).
[15]T. Driscoll, J. Quinn, M. Di Ventra, D. N. Basov, G. Seo, Y.-W. Lee, H.-T. Kim, and D. R. Smith, Phys. Rev. B **86**, 094203 (2012).
[16]J. Sakai, J. Appl. Phys. **103**, 103708 (2008).
[17]Y. Zhou, X. Chen, C. Ko, Z. Yang, C. Mouli, and S. Ramanathan, IEEE Electron Device Lett. **34**, 220–222 (2013).
[18]G. Stefanovich, A. Pergament, and D. Stefanovich, J. Phys.: Condens. Matter **12**, 8837 (2000).
[19]M. D. Pickett, G. Medeiros-Ribeiro, and R. S. Williams, Nat. Mater **12**, 114–117 (2013).
[20]S. Levitan, Y. Fang, D. Dash, T. Shibata, D. Nikonov, and G. Bourianoff, in *Proceedings of 13th International Workshop on Cellular Nanoscale Networks and Their Applications (CNNA)* (2012), pp. 1–6.
[21]A. Parihar, N. Shukla, S. Datta, and A. Raychowdhury, J. Appl. Phys. **117**, 054902 (2015).
[22]F. C. Hoppensteadt and E. M. Izhikevich, Phys. Rev. Lett. **82**, 2983–2986 (1999).
[23]S. Li, X. Liu, S. Nandi, D. Venkatachalam, and R. Elliman, in *Proceedings of 2014 Conference on Optoelectronic and Microelectronic Materials Devices (COMMAD)* (2014), pp. 138–140.
[24]P. E. Schmidt and R. C. Callarotti, J. Appl. Phys. **55**, 3144–3147 (1984).
[25]S. O. Pearson and H. S. G. Anson, Proc. Phys. Soc. London **34**, 204 (1921).

This article is copyrighted as indicated in the article. Reuse of AIP content is subject to the terms at: http://scitation.aip.org/termsconditions. Downloaded to IP: 130.56.107.13 On: Tue, 21 Jul 2015 08:47:01